Cured Poly(ethylene-g-maleic anhydride)/Graphene Nanocomposite: Properties and Characterization

B. Jafari[a], S. Hakim[a]*, M. Razavi-Nouri[b]

[a] *Iran Polymer and Petrochemical Institute, Polymerization Engineering Department, P.O. Box: 14975-112, Tehran, Iran.*
[b] *Iran Polymer and Petrochemical Institute, Polymer Processing Department, P.O. Box: 14975-112, Tehran, Iran.*

ABSTRACT

Poly(ethylene-g-maleic anhydride) (PEMA)/graphene nanoplatelets (xGn) (PEMA-xGn) composites were prepared by melt dispersion in an internal shear mixer. By adding dicumyl peroxide (DCP), cured poly(ethylene-g-maleic anhydride) C-PEMA was also produced. Different amounts of xGn were introduced into the PEMA in range of 0.5–5 wt. %. The effects of the sequence of feeding additives into the mixer on gel content, morphology, and mechanical properties allowed thermal, dynamic mechanical, and rheological behaviors to be studied. Results demonstrated that the incorporation of graphene into the polymer matrix decreased gel content and the rate of crosslinking. Scanning electron microscopy micrographs of the PEMA and C-PEMA nanocomposites showed that below 1 wt. % graphene, its dispersion in the matrix was desirable with no agglomerates.. Crystallization temperature increased due to heterogeneous nucleation by xGn. By curing the nanocomposites with DCP, crystallization temperatures decrease due to crosslinking and decreased crystallinity. The results of crosslinked nanocomposites revealed that, with the exception of C-PEMA containing 0.5 wt. % of xGn, mechanical properties decreased as xGn concentrations increased. Dynamic mechanical analysis showed that the increase of xGn in the PEMA matrix of up to 1 wt. % led to increased storage and loss modulus values. It was also revealed that α-transitions of the PEMA and α- and γ-transitions of C-PEMA were affected by polymer chain branching and graphene nanoplatelets. This could be attributed to interactions and potential bond formations between xGn and the maleic anhydride of PEMA. Rheological properties of the PEMA nanocomposites showed a quick change in the xGn fraction at about 1 wt. %.

1. Introduction

Linear low density polyethylene (LLDPE) has been developed rapidly due to a good balance between rigidity and strength and more flexible processing compared to low density or high density polyethylene (PE) [1]. PE is a commonly used polymer that can be chemically crosslinked to strengthen it for high performance applications [2]. The successful use of dicumyl peroxide (DCP) for crosslinking PE(XLPE) throughout the world, along with the capabilities of XLPE piping in cold- and hot-water envi-ronments, insulation for electrical cables, and for domestic water piping have generated significant interest and growth in the usage of these materials. What has made XLPE pipes so popular are the advantages they have over other piping materials, including 25-year lifespans, easy installation with fewer fittings, stability in corrosive environments, and resistance to biofilm build-up [2].

A new class of composite materials based on the incorporation of nanofillers has been investigated [3, 4]. Nanoscale materials often have unique properties (such as excellent thermal, electrical, and mechanical

---

properties) due to their small size [5]. The good dispersion of fillers in the matrix and their strong interfacial adhesion with polymers are usually essential elements needed to improve the mechanical performance of composites made from these materials [6].

There are several reports about polymer/graphene nanocomposites in the literature [7–9]. Kim et al. [1] prepared LLDPE/graphene nanocomposites and discussed the effect of PE functionalization and blending methods on graphene dispersion and composites properties. They reported nanocomposites prepared using a solution method, which provided better dispersion of graphene nanosheets in the polymer matrix and superior mechanical properties compared to nanocomposites prepared by melt mixing. Kim et al. [10] prepared master batch LLDPE/xGnP nanocomposites using solution compounding, and for better dispersion, compounding was carried out in a mini twin-screw extruder. The results showed that the tensile strength and modulus of composites dramatically increased with xGnP content.

UHMWPE-GNP nanocomposite films were prepared using an electrostatic powder-coating system [11]. The Young's modulus of UHMWPE-GNP nanocomposite films was higher than that of the neat UHMWPE. Zheng et al. [12] prepared HDPE-reinforced by expanded graphite and untreated graphite in a melt compounding process. Analysis of electrical properties showed that a rapid enhancement in electrical conductivity occurred when filler content exceeded 2 wt. %. The results also revealed that expanded graphite had lower percolation thresholds. Shen et al. [13] reported results associated with electrically conductive of PE/maleic anhydride grafted PE (g-PE)/EG prepared by solution intercalation and master batch melt mixing. Outcomes from electrical conductivity tests showed that samples prepared by solution intercalation had better electrical conductivity and lower percolation thresholds. In another work, LLDPE/xGnP was prepared by melt compounding [14], and xGnP was shown to increase the storage modulus and loss modulus over the entire temperature range. In a review paper, Morshedian et al. [15] mentioned that the incorporation of carbon black in the crosslinked PE reduced its gel content.

The main aim of this work was to discover the influence of xGn and DCP on mechanical and thermal properties and dynamic mechanical and rheological behaviors of dynamically cured PEMA nanocomposites. For this purpose, samples with various amounts of xGn (0, 0.5, 1, 2, and 5 wt. %) were prepared and cured with 0.5 wt. % of DCP.

Morphology, thermal and mechanical properties, and dynamic mechanical as well as rheological behavior of the uncured and cured nanocomposites were compared using scanning electron microscopy (SEM), differential scanning calorimetry (DSC), tensile measurements, dynamic mechanical analysis (DMA), and dynamic oscillatory rheometer, respectively. To the author's best knowledge, there is no study available that discusses the effect of graphene on the curing of PEMA by DCP, and no comparison has been made between the mechanical and thermal properties and rheological behavior of dynamically cured PE/graphene nanocomposites and uncured nanocomposites.

2. Materials and Methods

2.1. Materials

PEMA was supplied by the Karangin Company (1.7 % MA, Tm = 120°C, density = 0.92 g.cm⁻³ at 25°C) and used as the polymer matrix. Graphene nanoplatelets (xGn-C750) with 10% functional groups, including ethers, carboxyls, or hydroxyls, were provided by XG Sciences, Inc., USA. These groups reacted to atmospheric humidity to form acids or other compounds. DCP with 99% purity was purchased from Concord Chemical Ind. Co. Ltd (Taiwan).

2.2. Preparation of PEMA/xGn Nanocomposites

The PEMA and xGn were dried at 80°C for 12 h in a vacuum oven before being mixed. The dispersion of graphene in PEMA was done in an internal mixer (Brabender) at 150°C and at a rotor speed of 60 rpm for 11 min. At first, a master batch containing 5 wt. % graphene was prepared. The mixture was then diluted with a suitable amount of PEMA to prepare the nanocomposites containing 0.5, 1, and 2 wt. % graphene. The second step was accomplished at the same temperature and rotor speed but for 5.5 min. To cure the nanocomposites using a dynamic method, after mixing of the melt for 5.5 min, 0.5 wt. % DCP was added, and the nanocomposites cured for 3 min. Afterwards, the samples were compression molded by a Toyosiki hot press at 150°C at a pressure of 15 MPa for 5 min. The PEMA/xGn nanocomposites containing 0.5, 1, 2, and 5 wt. % xGn were designated as xGn-0.5, xGn-1, xGn-2, and xGn-5, respectively, and the cured samples were marked with a 'C'.

2.3. SEM

The cryofractured surfaces of unfilled and filled samples were gold sputter coated and observed using a VEGA SEM (Tescan Co., Czech Republic).

2.4. DSC

Thermal behavior of the samples was analyzed with a Netzsch-DSC 200F in a nitrogen atmosphere. Samples weighing 5 ± 0.1 mg were heated from room temperature to 170°C at a heating rate of 10°C/min and held at 170°C for 5 min to remove thermal history. The samples were then cooled and reheated to 170°C using the same rate.

2.5. Mechanical Properties

Tensile measurements were carried out with a universal test machine (Santam STM-20, Iran) according to the ISO 527-2 standard at a strain rate of 50 mm/min at 25 ± 2°C. At least five specimens were used to obtain an average value and standard deviation for each composition.

2.6. DMTA

Dynamic mechanical properties were measured by a DMTA (model: DMA 2000 Tritec, England). The samples were examined in a single cantilever bending mode at a frequency of 1 Hz, within a temperature range of -135 to 120°C and at a heating rate of 5°C/min.

2.7. Rheological Properties

Viscoelastic properties of the nanocomposites were measured using a stress controlled MCR300 rheometer at 150°C in a nitrogen atmosphere. The samples were tested using parallel plate geometry (φ = 25 mm) with a gap size of 1 mm. Dynamic strain sweep tests were first performed at a frequency of 1 rad/s to determine the linear viscoelastic region of the samples. Dynamic frequency sweep tests were then carried out within the linear viscoelastic region to evaluate the dynamic rheological properties of the samples (strain: 0.5%, angular frequency: 0.01 to 600 rad/s).

3.   Results and Discussion

The variation of torque as a function of mixing time for cured samples containing different graphene concentrations is shown in Figure 1. The first peak in the curves corresponds to the melting of PE. The second peak is related to the adding of DCP into the PE. This peak confirms that the curing reaction successfully took place [16]. Figure 1 shows that the incorporation of graphene reduced curing efficiency, but that graphene plays two crucial roles in the curing process. First, DCP attacks on PE chains reduced the degree of crosslinking due to graphene spatial obstacles. Second, graphene reduced the accessible gel

content, and a direct relationship existed between reductions of torque and gel content (Fig. 1). The measurement of gel content were performed by the xylene extraction (ASTM D2765) [17]. The obtained values were 65%, 61%, 59%, 55%, and 53% for neat C-PEMA, C-PEMA/0.5 wt. %, C-PEMA/1 wt. %, C-PEMA/2 wt. %, and C-PEMA/5 wt. % xGn, respectively.

3.1. Morphology

Figure 2A-E shows SEM images of fractured surfaces of the PEMA and PEMA nanocomposites. According to the datasheet, the average particle diameters of the xGn were calculated as 9.7 μm. In Fig. 2A, pure PEMA film has a smooth and continuous structure without cracks and pores. However, with incorporation of xGn nanoparticles into PEMA films, the roughness of the surface of the films increased. There were no significant agglomerates when the xGn concentrations increased to 1 wt. %, demonstrating that good dispersion of xGn can be obtained when lower concentrations of particles are used. Additionally, increases of more than 1 wt. % of xGn created poor dispersion and agglomerate formations of xGn in the PEMA. These results confirmed the enhancement of the mechanical performance of the nanocomposites at xGn concentrations up to 1 wt. % [18]. SEM images obtained of C-PEMA nanocomposites, presented in Figure 3A-E, show that a similar trend as uncured PEMA nanocomposites. Thus, it can be concluded that the curing process does not affect the dispersion of xGn in a polymer matrix.
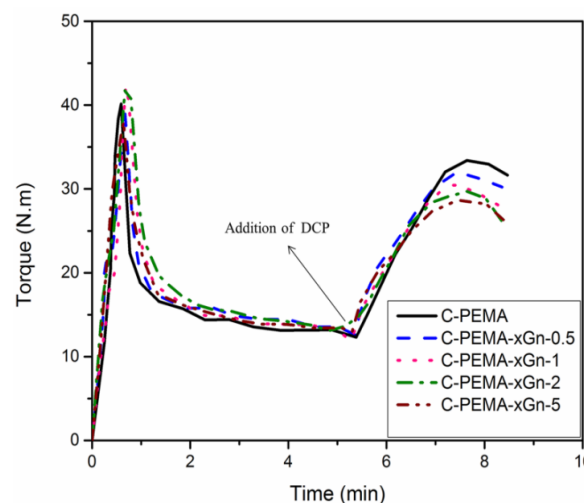

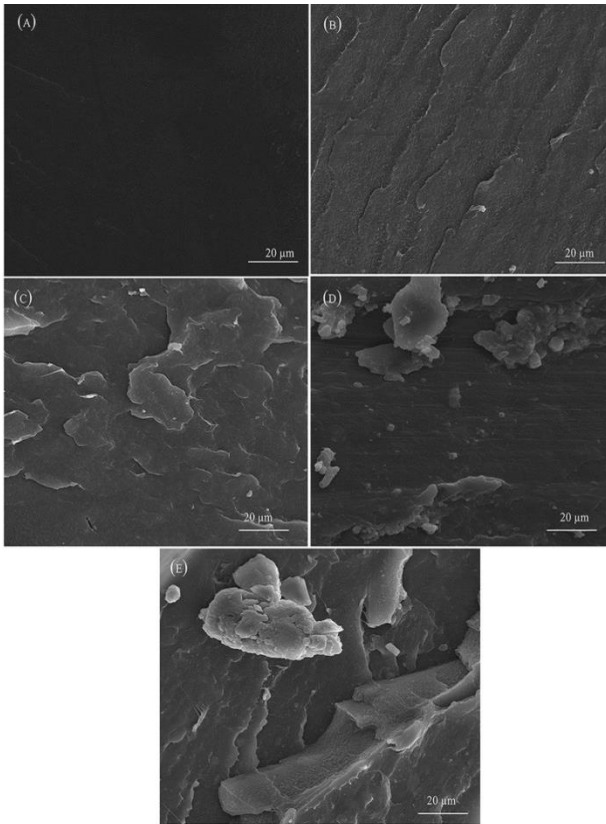**Figure 1.** Variation in torque with mixing times for C-PEMA

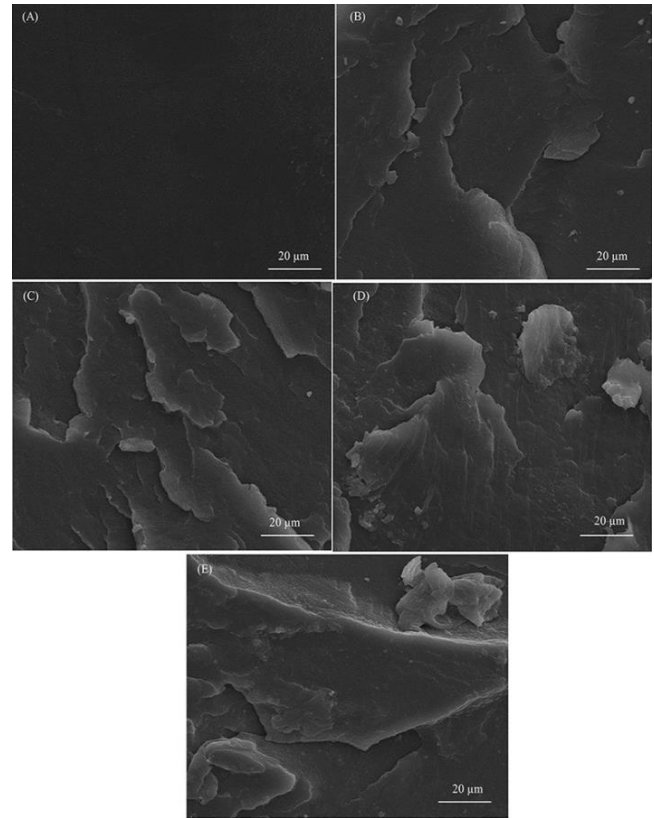**Figure 2.** SEM micrographs of (A) PEMA, (B) PEMA-xGn-0.5, (C) PEMA-xGn-1, (D) PEMA-xGn-2, and (E) PEMA-xGn-5

Figure 3. SEM micrographs of (A) C-PEMA, (B) C-PEMA-xGn-0.5, (C) C-PEMA-xGn-1, (D) C-PEMA-xGn-2, and (E) C-PEMA-xGn-5

Table 1. Crystallization, melting temperature, and degree of crystallinity of unfilled and filled materials

Sample	Temperature (°C)				$\Delta H_f (J.g^{-1})$	X_c (±2%)
	$T_{c\ onset}$	T_c	$T_{m\ onset}$	T_m		
PEMA	113.0	109.1	117.7	125.6	126.7	43.2
PEMA-xGn-0.5	116.0	112.0	115.6	127.1	121.9	41.6
PEMA-xGn-1	117.5	113.6	116.0	125.5	122.6	41.8
PEMA-xGn-2	117.5	112.8	115.7	127.1	127.2	43.4
PEMA-xGn-5	118.0	114.5	116.0	125.5	114.1	38.9
C-PEMA	115.4	109.9	103.5	125.6	103.8	35.4
C-PEMA-xGn-0.5	116.0	111.6	101.2	127.6	109.2	37.2
C-PEMA-xGn-1	116.0	111.9	101.4	126.3	110.1	37.5
C-PEMA-xGn-2	116.7	113.3	101.0	125.7	106.7	36.4
C-PEMA-xGn-5	117.5	114.3	101.9	124.7	105.3	35.9

3.2. Thermal Behavior

The heating and cooling thermograms of the PEMA and C-PEMA nanocomposites are presented in Figure 4A-D. The DSC results for crystallization peak temperature (T_c), melting peak temperature (T_m), onset temperature, heat of fusion (ΔH_f), and crystallinity (X_c) for PEMA and C-PEMA nanocomposites are summarized in Table 1. The crystallinity

(X_c) of the samples was also determined using the following equation:

$$X_c = \frac{\Delta H_f}{(1-\phi).\Delta H_f^*} \times 100 \qquad (1)$$

where ΔH_f is the theoretical enthalpy of fusion for a 100% crystalline PE with 293 J/g [19] and ϕ as the weight fraction of xGn in the sample.
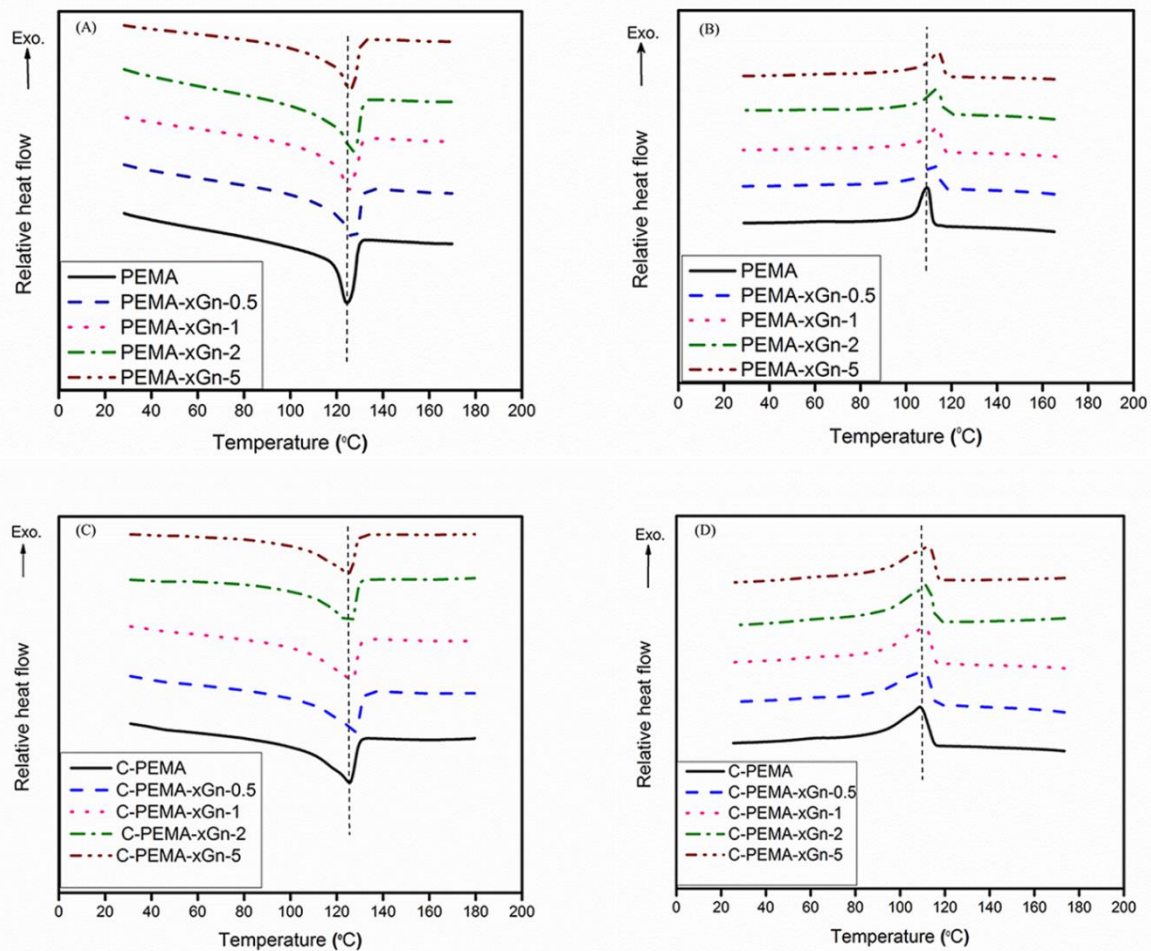
Figure 4. (A) DSC heating and (B) DSC cooling of unfilled and filled PEMA; (C) DSC heating and (D) DSC cooling of unfilled and filled C-PEMA

It was observed that, for PEMA and C-PEMA nano-composites, T_c and $T_{c\ onset}$ increased with the increase of xGn. This increase could be related to xGn generating heterogeneous nucleating sites for the crystallization of PEMA. However, Tm for PEMA nanocomposites did not change significantly by changing xGn content, but Tm onset slightly decreased [20–22]. The onset melting temperature of PEMA decreased after the formation of crosslinks. As shown in Table 1, the $T_{m\ onset}$ decreased from 117.7°C for PEMA to 103.5°C for C-PEMA, possibly due to reduced mobility of the PE chains [23]. Compared to the pure C-PEMA polymer matrix, onset melting temperatures of the nanocomposites were not significantly influenced by xGn addition, but the xGn slightly decreased the melting temperature. This could be attributed to the decrease of structural regularity of PEMA in the presence of xGn [16]. As can be seen in Table 1, the crystallinity of the nanocomposite samples remained approximately unchanged except for PEMA-xGn-5. The decrease in degree of crystallization of PEMA-xGn-5 in comparison to other nanocomposites could be related to the high concentration of xGn that hindered the chain mobility of crystallization [20].

3.3. Mechanical Properties

Tensile tests were performed to investigate the effect of nanosheet graphene loading on the mechanical properties of crosslinked nanocomposites and uncrosslinked PEMA. The variations of Young's moduli, tensile strength, elongation at break, toughness, and yield stress as a function of graphene content for PEMA and C-PEMA are shown in Figure 5A-D. In Figure 5A, the Young's modulus of the PEMA nanocomposites was significantly higher than that of the unfilled PEMA matrix.

For example, by adding 1 wt. % of xGn to a PEMA ma-trix, increased the Young's modulus from 116 to 180.3 MPa. The large surface area of xGn, good dispersion, strong interfacial adhesion, and formation of hydrogen bonding between the polar groups of PEMA and xGn are significant parameters [1, 24]. With an increase of more than 1 wt. % of xGn, the Young's modulus decreased, possibly due to the agglomeration of xGn in the PEMA polymer matrix. The peak in the Young's modulus curve could be seen at 0.5 wt. % for C-PEMA nanocomposites. To validate this phenomenon, gel content results can be used as evidence because graphene greatly affects the curing

efficiency [24, 25]. Figure 5B shows that xGn incorporation also led to an increase in the tensile strength values to a maximum of 19.5 MPa for the PEMA nanocomposite with 1 wt. % xGn. In this case, graphene nanosheets not only crosslinked to the polymer chains temporarily but also provided regions of enhanced strength that mitigated crack or cavity formation. Energy dissipation could be improved by the presence of mobile crystallites [26]. With an increase of more than 1 wt. % xGn, tensile strength started to decrease. Interfacial adhesion was reduced at 2 and 5 wt. % xGn due to formation of agglomerates, which in turn decreased tensile strength [27]. Tensile strength increased from 16.7 to 23 Mpa for C-PEMA nanocomposites containing 0.5 wt. % graphene. As the percentage of graphene became greater than 0.5%, a descending trend in tensile strength was observed. The decrease in tensile strength of C-PEMA-xGn-5 in comparison to other nanocomposites could be related to the effect of graphene on curing and creating stress cracks or cavities.

The elongation at break of the nanocomposite slightly decreased by adding 0.5 wt. % of xGn to PEMA (Fig. 5C), which could be related to the layered nanoparticle surfaces bonding with each other to create the entangled surface. Moreover, the small decrease in the elongation at break for the PEMA nanocomposites (containing 1, 2, and 5 wt. % of xGn) compared to the pure matrix was noticeable. Decreases in strain at break was only 1% for the 2 wt. % xGn sample compared to the PEMA. For the 5 wt. % xGn sample, decrease in strain at break was about 12%. Most of these results show that the small decreases in failure strain do not significantly affect the strength of the PEMA-xGn nanocomposites when using graphene loading [28]. A significant decrease in elongation at break was observed from 1060% in PEMA to 380% in the C-PEMA as a result of crosslink formation between the chains of PEMA as shown in Figure 5C. With the exception of C-PEMA containing 0.5 wt. % of xGn, the strain at break of C-PEMA nanocomposites decreased as xGn concentrations increased, which coincided with the results obtained from the SEM images [29].
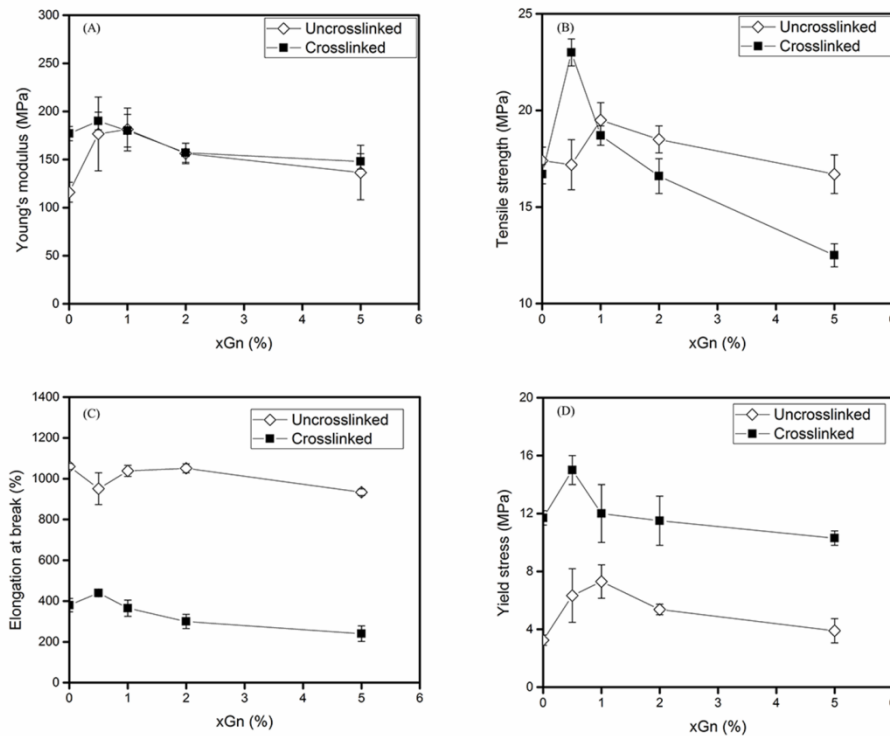

Figure 5. Mechanical properties of uncrosslinked and crosslinked nanocomposites: (A) Young's modulus, (B) tensile strength, (C) elongation at break, and (D) yield stress of unfilled and filled PEMA and C-PEMA with different xGn content

Figure 5D shows that the yield stress had a similar trend as the Young's modulus. The yielding process was extremely material dependent, being related directly to molecular mobility [30]. The maximum improvement in yield stress was 7.3 MPa at 1 wt. % xGn, compared to 3.25 MPa in PEMA. This can be attributed to the strong interactions between the matrix and the graphene nanosheets that reduced mobility of polymer segments and increased the resistance to motion of the polymer chains under stress. Increased graphene, especially at 5 wt. %, due to the reduction of interfacial interactions between the polymer matrix and graphene nanosheets, caused resistance polymer chain movement, leading to decreased yield stress. A significant enhancement to yield stress was observed in C-PEMA compared to PEMA, attributed to the creation of crosslinks between the C-PEMA chains and hardening of the movements of the polymer chains. For 0.5 wt. % loading of xGn, yield stress reached a maximum of 15 MPa, compared to C-PEMA (11.7 MPa) and then decreased

3.4. Dynamic Mechanical Properties

Dynamic mechanical properties for PEMA and C-PEMA nanocomposites were obtained in terms of storage modulus (E′) and loss modulus (E″) which are shown in Figs. 6A-B. Figure 6A shows that the E′ increased with the increase in xGn up to 1 wt. %,

which could be due to the large surface area of xGn, good interfacial adhesion, and the formation of hydrogen bonding between the polar groups of PEMA and xGn. With an increase of graphene of more than 1 wt. %, the E′ decreased, and its value for PEMA-xGn-5 was lower than that of PEMA at the studied temperature range. The observed phenomenon could be related to the existence of higher amounts of graphene particles in comparison to that of MA groups in PEMA [31, 32]. This could have a negative effect on the adhesion of graphene to PEMA and its dispersion in the matrix.

Figure 6B shows that the E″ increased with the increase of xGn content in PEMA nanocomposites. For the composites filled with the particles, the matrix can be divided into two parts: the free part, in which the state of molecular chains is the same as in the pure matrix and the bound part, namely the mesophase, which is formed by the physical or chemical adsorption of the chains and transcrystallization on the filler surface [25]. When the composites are subjected to external stress, the external energy is dissipated by particle–particle and particle–matrix friction in the mesophase, in which the loss modulus increased [25]. The lowest E″ value was obtained for PEMA-xGn-5 and attributed to higher amounts of xGn compared to those of the MA groups in PEMA. This decreased particle–particle and matrix–particle interactions [25].
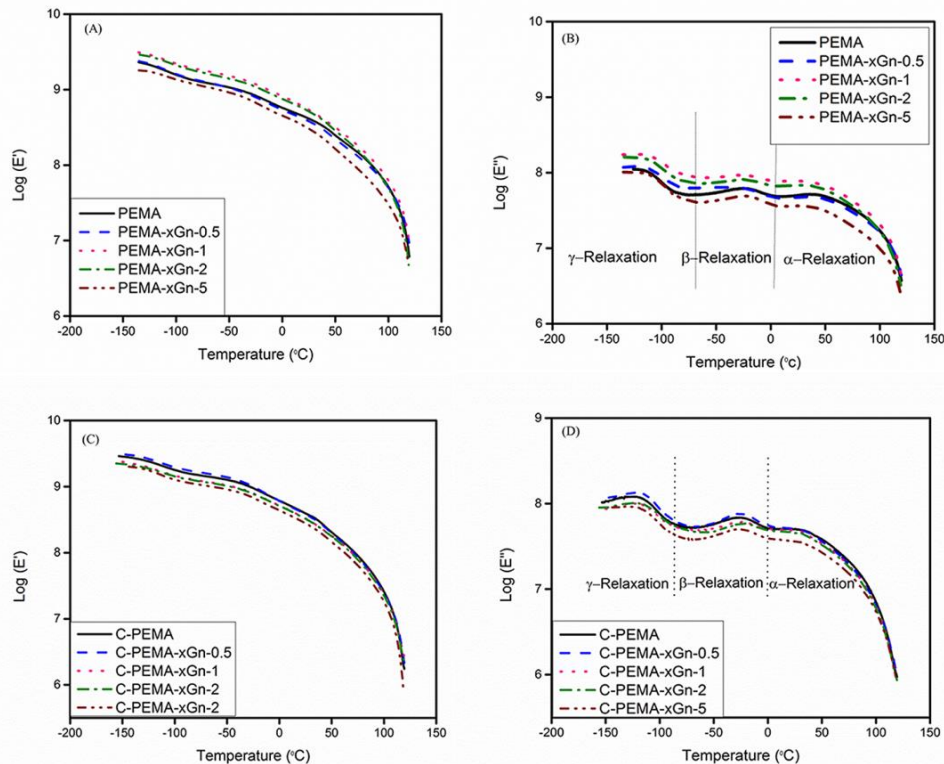

Figure 6. Dynamic mechanical curves for PEMA–xGn (A) E′, (B) E″ and C-PEMA-xGn, (C) E′, and (D) E″

Figure 6C shows the storage modulus of the C-PEMA nanocomposite, which was higher than that of PEMA at -135°C because of crosslinking. By the addition of only 0.5 wt. % of xGn, the storage modulus of the nanocomposite at -135°C increased from 2634 to 2891 Mpa, which is attributed to the large surface area to volume ratio of xGn, good interfacial adhesion, and creation of hydrogen bonds between polar groups of PEMA and xGn. With the increase of graphene over 0.5% a decline in the storage modulus was observed, caused by the influence of graphene on curing [25]. The E″ of the C-PEMA nanocomposite increased with the increase of xGn up to 0.5 wt. % (Fig. 6D). With an increase of graphene more than 0.5 wt. %, the E″ decrease because of higher amounts of graphene particles that decrease the crosslink density (Figure 1) and particle–particle and matrix–particle interactions.

Dynamic mechanical analysis of PE prior to melting showed three peaks, termed α-, β-, and γ-transitions [33]. The α-peak appeared between 20 and 60°C for the studied PE [34], which is usually representative of the crystalline phase [34]. The β-peak was observed between -5 and -35°C. Khanna et al. [35] demonstrated that the β-peak in PE is the glass transition temperature (T_g). The ɤ-peak is observed between -100 and -125°C and includes motion of the short segments (three to four methylene groups) of the amorphous phase [35]. Figure 6B indicates that the α-transition peak of the PEMA nanocomposites filled with xGn shifted to lower temperatures in comparison to PEMA alone. It was observed that the peak temperature of the α-transition decreased 15°C for PEMA-xGn-5 compared to the pristine matrix, which could be related to the reduction of crystallinity for the nanocomposite [25]. However, the position of the β- and γ-transition peaks of the PEMA nanocomposites remained unchanged. From the DMTA thermograms, the γ- and α -transitions for C-PEMA nanocomposites were influenced by distribution of xGn in the surrounding matrix. The γ-transition peak shifted to higher temperatures with increases in the graphene content and reached a maximum at a graphene content of 2 wt. % before decreasing. This was attributed to the motions of the CH2 units in the amorphous region [36]. The α-transition peaks in the C-PEMA nanocomposites shifted to lower temperatures with increases in graphene content, which was attributed to the integrity loss of C-PEMA crystallites that resulted in more crystal defects [37]. Therefore, the γ-transition for C-PEMA nanocomposites were -123.5, -122.5, -122.3, -119, and -126°C, and the α–transition were 35, 35, 31.7, 31, and 30.5°C for neat C-PEMA, C-PEMA-0.5 wt. % xGn, C-PEMA-1 wt. % xGn, C-PEMA-2 wt. % xGn, and C-PEMA-5 wt. % xGn,

respectively. The position of the β- transition peak remained unchanged.

3.5. Rheology

Dynamic rheological measurements were also used to investigate the rheological behavior of the PEMA and C-PEMA nanocomposites with various xGn loadings. The storage modulus (G') and loss modulus (G'') of the PEMA and C-PEMA nanocomposites with different xGn content as a function of frequency are shown in Figure 7A-D. G' of PEMA and C-PEMA nanocomposites increased with an increase in the angular frequency. When xGn content was equal or more than 1 wt. %, the flow regime of PEMA-xGn nanocomposites was significantly altered at low frequencies in terminal regions, and a pseudosolid like behavior was observed [18, 38]. The G' of C-PEMA nanocomposites decreased with increases of xGn loading, due to the hindering effect of graphene on curing efficiency. The loss modulus (G'') of the PEMA and C-PEMA nanocomposites showed a similar tend as G', and Figures 7A and 7B show that the increase in the G' of the PEMA-xGn nanocomposites was greater than that of the G'' in the specified frequency. Thus, the effect of xGn on rheological behavior of PEMA is more sensitively reflected on the G' compared to the G''. Figures 8A and 8B show complex viscosity |η^*| of the PEMA and C-PEMA nanocomposites with different xGn loadings. PEMA-xGn-5 nanocomposites exhibited a very strong shear thinning behaviour, whereas PEMA behaved like a Newtonian fluid. These observations indicate the transition from a liquid-like to a solid-like viscoelastic behavior [38, 39]. The effect of xGn on the rheological behavior of the nanocomposites was studied using the power-law relationship [19];

$$\eta^* = m \left| \omega \right|^{n-1}, \tag{2}$$

where η^* is the complex viscosity, ω is the angular frequency, n is the power-law index, and m is a constant. Table 2 shows that the value of n for uncrosslinked PEMA nanocomposites is lower compared to that of PEMA. A vice-versa trend was observed for the crosslinked samples. The slopes of the terminal zones of the G' and G'' and power-law index (n) are also given in Table 2, and G' and G'' of the PEMA-xGn-5 nanocomposites nearly become independent of frequency in the low ω region. The rheological measurements for crosslinked samples over the studied range of frequencies showed less variation of G', G'', and |η^*| compared to ω in the uncross-linked samples. This conflict was caused by increasing xGn, which led to increased interfacial adhesion and formation of H-bonding between the xGn and polymer. The increase of graphene nanosheets reduced the curing efficiency

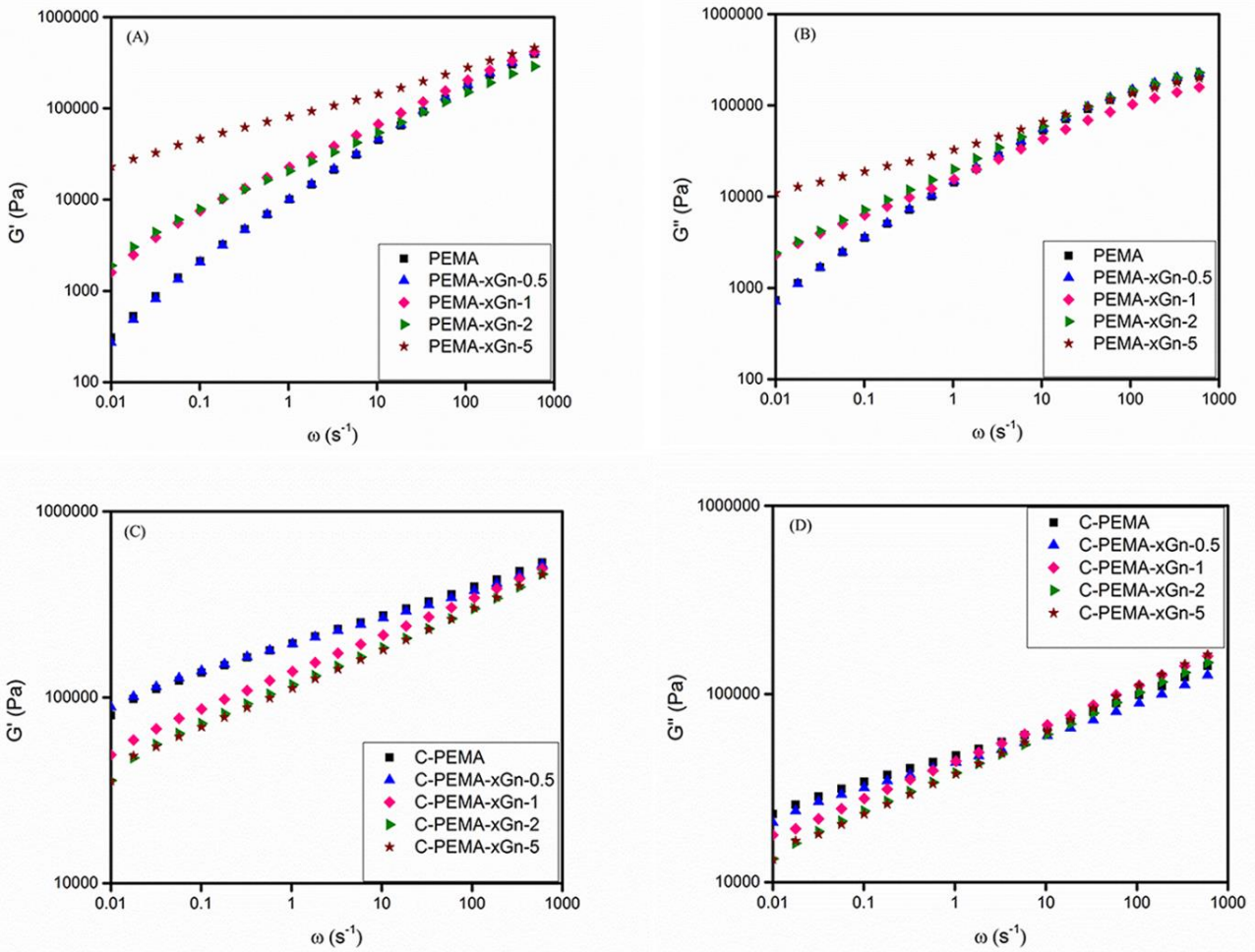and percentage of crosslinking and decreased melt strength.

Figure 7. (A) G' and (B) G'' of unfilled and filled PEMA; (C) G' and (D) G'' of unfilled and filled C-PEMA with different xGn contents at 150˚C

Table 2. The slopes of terminal zones for G' and G" and the power-law index for the unfilled and filled materials

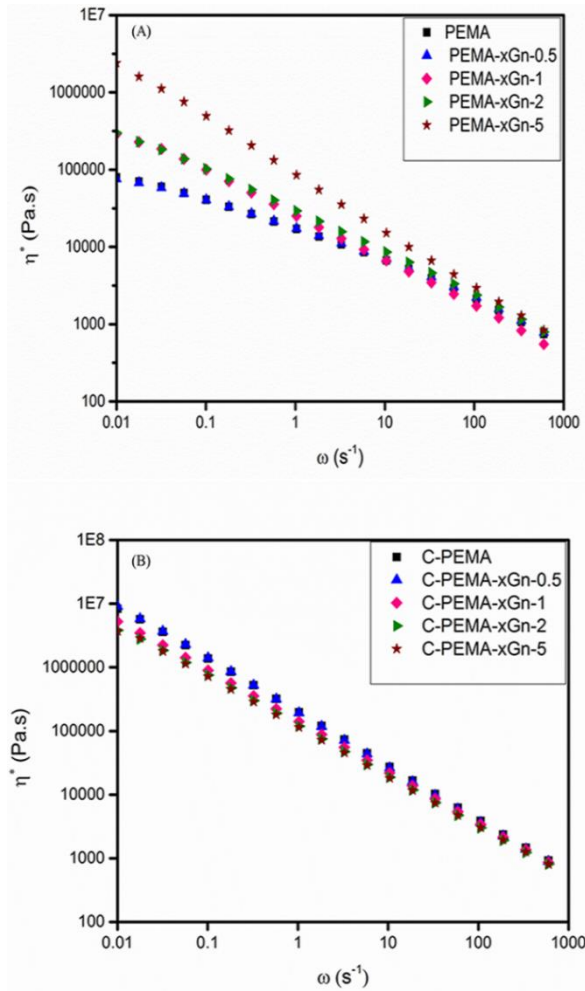| Sample	slope of G' vs.ω (± 0.02)	slope of G'' vs. ω (± 0.02)	power law index (± 0.01)
PEMA	1.71	1.53	0.51
PEMA-xGn-0.5	1.77	1.55	0.51
PEMA-xGn-1	1.59	1.33	0.44
PEMA-xGn-2	1.56	1.33	0.41
PEMA-xGn-5	1.21	1.16	0.28
C-PEMA	1.22	1.12	0.15
C-PEMA-xGn-0.5	1.13	1.07	0.15
C-PEMA-xGn-1	1.20	1.14	0.19
C-PEMA-xGn-2	1.32	1.21	0.21
C-PEMA-xGn-5	1.36	1.24	0.22

Figure 8. (A) Complex viscosity of unfilled and filled PEMA; (B) complex viscosity of unfilled and filled C-PEMA with different xGn contents at 150℃

4. Conclusion

Nanocomposites of PEMA-xGn and cured PEMA-xGn were prepared using a melt-mixing method. The morphology, thermal, and mechanical properties, as well as dynamic mechanical and rheological behaviour, of the PEMA-xGn and cured PEMA-xGn nanocomposites with different amounts of xGn were investigated. The results showed that the increase of graphene decreased gel content. Mechanical tests showed that incorporation of xGn significantly improved the Young's modulus, tensile strength, and yield stress of the PEMA matrix up to 1 wt. %. The elongation at break was not significantly changed; however, the mechanical properties of C-PEMA nanocomposites decreased as xGn concentration increased except for C-PEMA containing 0.5 wt. % of xGn. SEM observations showed uniform dispersion of xGn throughout the matrix up to 1 wt. %, and a stark fractured nanocomposite surface, which were evidences of the remarkable enhancements in overall mechanical properties. The crystallization behavior

of PEMA in the presence of xGn showed that it behaved as a heterogeneous nucleating agent. DMTA results for PEMA nanocomposites showed a similar trend to mechanical properties. The substantial reinforcing effect of xGn up to the optimal loading (1 wt. %) were observed, possibly due to interactions between xGn and the polymer. Meanwhile the E' and E'' of C-PEMA/xGn nanocomposites both decreased with the increase of xGn, except for C-PEMA containing 0.5 wt. % graphene. Dynamic rheological measurements revealed that storage and loss modulus of PEMA as a function of angular frequency increased with increased xGn loading. The PEMA-xGn nanocomposites containing 5 wt. % of xGn exhibited a very strong shear thinning behavior whereas the PEMA almost behaved like a Newtonian fluid. Furthermore, reduced rheological parameters of C-PEMA nanocomposites (G', G'', and η^*) compared to that of C-PEMA were achieved by addition of xGn.

References

[1] Kim H, Kobayashi MA, Abdurrahim MJ, Zhang A, Khusainova MA, Hillmyer MA, Abdala AA, Macosko CW. Graphene/Polyethylene Nanocomposites: Effect of Polyethylene Functionalization and Blending Methods. *Polymer* 2011; 52: 1837–1846.

[2] Yamazaki T, Seguchi T. ESR Study on Chemical Crosslinking Reaction Mechanisms of Polyethylene Using a Chemical Agent. *J Polym Sci part-A Polym Chem* 1997; 35: 279–284.

[3] Thostenson ET, Ren Z, Choua TW. Advances in the Science and Technology of Carbon Nanotubes and Their Composites: a Review. *Compos Sci Technol* 2001; 61: 1899–1912.

[4] Lebaron PL, Wang Z, Pinnavaia TJ. Polymer-Layered Silicate Nanocomposites: an Overview. *J Appl Clay Sci* 1999; 15: 11–29.

[5] Chivrac F, Pollet E. Av´erous L. Progress in Nano-Biocomposites Based on Polysaccharides and Nanoclays. *Mater Sci Eng R* 2009; 67: 1–17.

[6] Kim H, Abdala AA, Macosko CW. Graphene/Polymer Nanocomposites. *Macromolecules* 2010; 43: 6515–6530.

[7] Kuilla T, Bhdra S, Yao D, Kim NH, Bose S, Lee JH. Recent Advances in Graphene Based Polymer Composites. *Prog Polym Sci* 2010, 35: 1350–1375.

[8] Potts JR, Dreyer DR, Bielawski CW, Rouff RS. Graphene-Based Polymer Nanocomposites. *Polymer* 2011; 52: 5–25.

[9] Das TK, Prusty S. Graphene-Based Polymer Composites and Their Applications. *Polym Plast Technol Eng* 2013; 52: 319–331.

[10] Kim S, Do I, Drzal LT. Multifunctional xGnP/LLDPE Nanocomposites Prepared by Solution Compounding Using Various Screw Rotating Systems. *Macromol Mater Eng* 2009; 294: 196–205.

[11] Lahiri D, Dua R, Zhang C, Socarraz-Novoa I D, Bhat A, Ramaswamy S, Agarwal A. Graphene Nanoplatelet-Induced Strengthening of Ultrahigh Molecular Weight Polyethylene and Biocompatibility in Vitro. *Am Chem Soc* 2012; 4: 2234–2241.

[12] Zheng W, Lu X, Wong SC. Electrical and Mechanical Properties of Expanded Graphite-Reinforced High-Density Polyethylene. *J Appl Polym Sci* 2004; 91: 2781–2788.

[13] Shen JW, Huang WY, Zuo SW, Hou J. Polyethylene/Grafted Polyethylene/Graphite Nanocomposites: Preparation, Structure, and Electrical Properties. *J Appl Polym Sci* 2005; 97: 51–59.

[14] Kim S, Do I, Drzal LT. Thermal Stability and Dynamic Mechanical Behavior of Exfoliated Graphite Nanoplatelets-LLDPE Nanocomposites. *Polym Compos* 2010; 31: 755–761.

[15] Morshedian J, Mohammad Hoseinpour P. Polyethylene Cross-Linking by Two-Step Silane Method: a Review. *Iran Polym J* 2009; 18: 103–128.

[16] Azizi H, Morshedian J, Barikani M, Wagner MH. Effect of Layered Silicate Nanoclay on the Properties of Silane Crosslinked Linear Low-Density Polyethylene (LLDPE). *Express Polym Lett* 2010; 4: 252–262.

[17] ASTM D2765-01. Standard Test Methods for Determination of Gel Content and Swell Ratio of Crosslinked Ethylene Plastics, Annual Book of ASTM Standards, 8.01, 2006.

[18] Yang X, Zhan Y, Zhao R, Liu X. Effects of Graphene Nanosheets on the Dielectric, Mechanical, Thermal Properties, and Rheological Behaviors of Poly(arylene ether nitriles). *App Polym Sci* 2012; 124: 1723–1730.

[19] Razavi-Nouri M, Karami M. Effect of Rubber Content on Morphology and Thermal and Rheological Behaviors of Acrylonitrile-Butadiene Rubber/Poly(ethylene-co-vinyl acetate)/Organoclay Nanocomposites. *Polymer* 2014; 55: 6940–6947.

[20] Shanks RA, Cerezo FT. Preparation and Properties of Poly(propylene-g-maleic anhydride) Filled with Expanded Graphite Oxide. *Compos Part A- Appl S* 2012; 43: 1092–1100.

[21] Cheng S, Chen X, Grace Hsuan Y, Li CY. Reduced Graphene Oxide-Induced Polyethylene Crystallization in Solution and Nanocomposites. *Macromolecules* 2011; 45: 993–1000.

[22] Lai SM, Chen WC, Wang ZW. Effectiveness of a Maleated Compatibilizer on the Tensile and Tear Properties of Peroxide-Cured Metallocene Polyethylene/Clay Nanocomposites. *J Polym Res* 2010; 18: 1033–1042.

[23] Kim DH, Kim SC. Dicumyl Peroxide-Initiated Crosslinking Reaction of Low Density Polyethylene. *Polym Korea* 1984; 8: 44–52.

[24] Lee C, Wei X, Keysar WJ, Hone J. Measurement of the Elastic Properties of Intrinsic Strength of Monolayer Graphene. *Science* 2008; 321: 385–388.

[25] Huang Y, Jiang S, Wu L, Hua Y. Characterization of LLDPE/Nano-SiO2 Composites by Solid-State Dynamic Mechanical Spectroscopy. *Polym Test* 2004; 23: 9–15.

[26] Kontou E, Niaounakis M. Thermo-Mechanical Properties of LLDPE/SiO2 Nanocomposites. *Polymer* 2006; 47: 1267–1280.

[27] Roumeli E, Pavlidou E, Avgeropoulos A, Vourlias G, Bikiaris DN, Chrissafis K. Factors Controlling the Enhanced Mechanical and Thermal Properties of Nanodiamond-Reinforced Cross-Linked High Density Polyethylene. *J Phys Chem B* 2014; 118: 11341–11352.

[28] Durmus A, Kasgöz A, Macosko C. Mechanical Properties of Linear Low-Density Polyethylene (LLDPE)/Clay Nanocomposites: Estimation of Aspect ratio and Interfacial Strength by Composite Models. *J Macromol Sci Part B* 2008; 47: 608–619.

[29] Antunes M, Gelder G, Velasco JI. Multifunctional Nanocomposite Foams Based on Polypropylene with Carbon Nanofillers. *J Cell Plast* 2013; 49: 259–279.

[30] Roylance D. Yield and Plastic Flow, Mechanics of Matherials. Department of Materials Science and Engineering Massachusetts Institute of Technology, Cambridge, MA, 2001.

[31] Vallés C, Kinloch IA, Young RJ, Wilson NR, Rourke JP. Graphene Oxide and Base-Washed Graphene Oxide as Reinforcements in PMMA Nanocomposites. *Compos Sci Technol* 2013; 88: 158–164.

[32] Salarbashi D, Noghabi MS, Bazzaz BSF, Shahabi-Ghahfarrokhi I, Jafari B, Ahmadi R. Eco-Friendly Soluble Soybean Polysaccharide/Nanoclay Na+ Bionanocomposite: Properties and Characterization. *Carbohyd Polym* 2017; 169: 524–532.

[33] Sha H, Zhang X, Harrison IA. Dynamic Mechanical Thermal Analysis (DMTA) Study of Polyethylenes. *Thermochim Acta* 1991; 192: 233–242.

[34] Khanna YP, Turi EA, Taylor TJ, Vickroy VV, Abbott RF. Dynamic Mechanical Relaxations in Polyethylene. *Macromolecules* 1985; 18: 1302–1309.

[35] Hoffman JD, Williams G, Passaglia E. Analysis of the α, β and γ Relaxations in Polychlorotrifluoroethylene and Polyethylene : Dielectric and Mechanical Properties. *J Polym Sci Part C: Polym Sym* 1966; 14: 173–235.

[36] Lew CY, Murphy WR, Mcnally GM. Preparation and Properties of Polyolefin-Clay Nanocomposites. *Polym Eng Sci* 2004; 44: 1027–1035.

[37] Mokoena MA, Djokovi´c V, Luyt AS. Composites of Linear Low Density Polyethylene and Short Sisal Fibres: the Effects of Peroxide Treatment. *J Mater Sci* 2004; 39: 3403–3412.

[38] Zhang HB, Zheng WG, Yan Q, Jiang ZG, Yu ZZ. The Effect of Surface Chemistry of Graphene on Rheological and Electrical Properties of Polymethylmethacrylate Composites. *Carbon* 2012; 50: 5117–5125.

[39] Valentino O, Sarno M, Rainone NG, Nobile MR, Ciambelli P, Neitzert HC, Simon GP. Influence of the Polymer Structure and Nanotube Concentration on the Conductivity and Rheological Properties of Polyethylene/CNT Composites. *Physica E 2008*; 40: 2440–2445.